Blue afterglow emission of glass-ceramics synthesized by melting mixture of ZrO_2:Ti, K_2CO_3, and H_3BO_3

Susumu Nakayama (Department of Applied Chemistry and Biotechnology, National Institute of Technology (KOSEN), Niihama College, s.nakayama@niihama-nct.ac.jp, Japan)
Masaki Shiomi (Engineering Design Education Center, KOSEN, Niihama College, m.shiomi@niihama-nct.ac.jp, Japan)

Abstract

This study investigates the enhancement of blue afterglow emission from ZrO_2:Ti heat treatment at 1500 °C in air with raw ZrO_2 containing 1000 ppm TiO_2. The afterglow time of $KZrB_4O_{8.5}$, which was melt heat-treated with ZrO_2:Ti heat-treated at 1500 °C, K_2CO_3, and H_3BO_3 at 1300 °C in air, was extended by approximately 2.5 times. XRD analysis of ZrO_2:Ti revealed only monoclinic peaks, while that of $KZrB_4O_{8.5}$ with a glass-ceramic composition displayed monoclinic peaks and a halo. In the XPS analysis of ZrO_2:Ti and $KZrB_4O_{8.5}$ with a glass-ceramic composition, the presence of Zr^{4+} and a small amount of Zr^{3+} was observed, while that of Zr^{2+} could not be confirmed. SEM observations revealed that ZrO_2:Ti was composed of uniformly sized grains of approximately 0.5 μm size, whereas $KZrB_4O_{8.5}$ with a glass-ceramic composition exhibited coarsened grains of approximately 10 μm size. The afterglow decay curves of $KZrB_2O_{5.5}$, $KZrB_3O_{7.0}$, $KZrB_5O_{10.0}$, and $KZrB_6O_{11.5}$ with a glass-ceramic composition with varying B content in $KZrB_4O_{8.5}$ with a glass-ceramic composition were measured, and based on the results obtained, the afterglow time increased with an increase in the coarse grain size.

Key words

photoluminescence, monoclinic zirconia, X-ray diffraction, X-ray photoelectron spectroscopy, scanning electron microscope

1. Introduction

Zirconia (ZrO_2) phosphors are known to produce blue fluorescence without the need for expensive rare earth luminescent elements (Akiyama et al., 2002). When a small amount of titanium (Ti) is solidly dissolved in this ZrO_2 phosphor, strong fluorescence is observed (Iwasaki et al., 2018; Kuboyama et al., 2018). In this study, we extensively investigated the relationship between the amount of Ti solid solution and fluorescence intensity in the ZrO_2 phosphor, as well as the enhancement of fluorescence intensity by the solid dissolution of a third component. When 1000 ppm of Ti and 5000 ppm of phosphorus (P) are dissolved, a very strong blue fluorescence is obtained with absorptivity, internal quantum yield, and external quantum yield of 53 %, 59 %, and 31 %, respectively (Nakayama et al., 2016; Nakayama et al., 2016). ZrO_2 phosphors are also known to exhibit long afterglow properties (Akiyama et al., 2002). For example, studies have reported that the formation of Zr^{2+} and the associated formation of oxygen defects affect the long afterglow properties of high-purity ZrO_2 (Shimizu et al., 1999). The long afterglow property of ZrO_2:Ti has also been reported to improve by a change in Ti valence from +4 to +3 (Cong et al, 2007; Wang et al., 2012). Furthermore, ZrO_2:0.1%Ti heat-treated at 1500 °C reportedly has a higher photoluminescence (PL) peak intensity and longer afterglow time than that heat-treated at 1200 °C (Shimizu et al., 1999). Therefore, in this study, we used ZrO_2:Ti as the material, which was heat-treated at 1500 °C. However, in the practical phosphorescent material $SrAl_2O_4$: Eu^{2+}, Dy^{3+}, the growth of secondary particle size and smoothing of the grain surface has been reported to enhance the afterglow property (Hai et al., 2016; Kuboyama et al., 2018). When ZrO_2 is composited with glass, the flux effect can be expected to cause the crystal particle size of ZrO_2 to grow. By using ZrO_2:Ti, heat treatment at high temperature, and coarsening the crystal grains as described above, the afterglow time of monoclinic ZrO_2 can be extended. In this study, we attempted to enhance the long afterglow property of ZrO_2:Ti via composite treatment with potassium borate glass.

2. Experimental procedure

The raw material used in this study was ZrO_2 powder (SPZ-grade, Daiichi Kigenso Kagaku Kogyo Co. Ltd.) with a monoclinic crystal structure. The impurity TiO_2 content was approximately 0.1 wt%. Additionally, other impurities included SiO_2 (0.030 wt%), Fe_2O_3 (0.002 wt%), and P_2O_5 (0.030 wt%). The powder obtained by heat-treating the ZrO_2 powder in an alumina crucible (SSA-S, Nikkato Co.) at 1500 °C for 2 h was referred to as ZrO_2:Ti. Special grade reagents K_2CO_3 and H_3BO_3 purchased from Fujifilm Wako Pure Chemical Co., were blended with ZrO_2:Ti to create a $KZrB_4O_{8.5}$ composition. The mixture was then mixed in a mortar for 1 h, packed in an alumina crucible, melted at 1300 °C for 5 h in an air atmosphere, and allowed to cool in an electric furnace to obtain a bulk body of $KZrB_4O_{8.5}$ with a glass-ceramic composition. Finally, the prepared ZrO_2:Ti and $KZrB_4O_{8.5}$ with a glass-ceramic composition were pulverized using a zirconia mortar.

The emission spectra, excitation spectra, and afterglow

decay curves of the samples were measured using a spectrofluorophotometer (FP-6500, JASCO Co.). Afterglow decay measurements were performed by irradiating excitation light of 285 nm for 60 s, stopping the irradiation of excitation light, and continuously measuring the fluorescence of 475 nm at intervals of 0.1 s. The sample powders were analyzed using an X-ray diffractometer (XRD, MiniFlex II, Rigaku Co.) with a CuKα radiation source and a graphite monochromator. X-ray photoelectron spectroscopy (XPS) analyses of the electronic states of Zr*3d* were performed using a Kratos AXIS-ULTRA system (Shimadzu Co.) with an AlKα radiation source. For the XPS measurements, the samples were kept in a vacuum chamber (*ca* 1×10^{-5} Pa). A neutralizing gun was used to prevent charge buildup. The O1s peak was calibrated to 531.6 eV for accuracy. The measurements were repeated eight times to ensure data accuracy. Kratos software Vision2 was used for fitting and deconvolution. An analysis of the sample was performed using a scanning electron microscope (SEM; JSM-7500F, JEOL Ltd.) equipped with an energy-dispersive detector (EDS; JED-2300F, JEOL Ltd.).

3. Results and discussion

The emission and excitation spectra of ZrO_2:Ti and $KZrB_4O_{8.5}$ with a glass-ceramic composition are presented in Figure 1. The emission spectra, which were measured using 280 nm excitation light, exhibited a broad emission peak ranging from 420 to 620 nm with a maximum intensity at 475 nm.

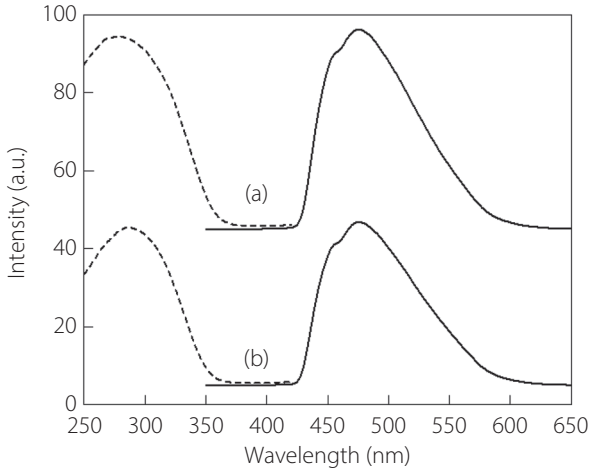

Figure 1: Excitation (left, emission: 475 nm) and emission (right, excitation: 280 nm) spectra

Note: (a) ZrO_2:Ti and (b) $KZrB_4O_{8.5}$ with a glass-ceramic composition.

Figure 2 show the afterglow decay curves of ZrO_2:Ti and $KZrB_4O_{8.5}$ with a glass-ceramic composition. The afterglow decay curve of $KZrB_4O_{8.5}$ with a glass-ceramic composition showed a slight difference in the fluorescence intensity immediately after the excitation light irradiation was terminated. The afterglow time was defined as the point where the

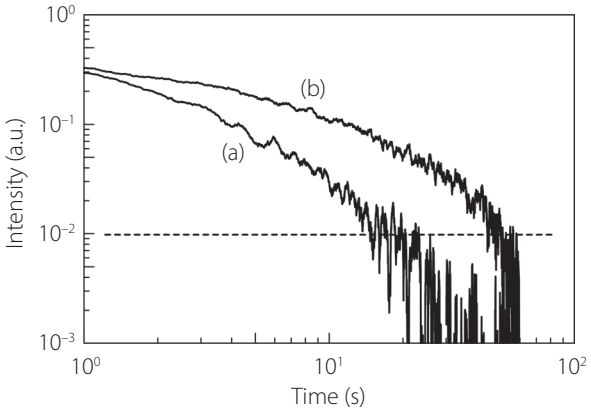

Figure 2: Afterglow decay curves at 475 nm measured by excitation at 280 nm (exposure time: 1 min)

Note: (a) ZrO_2:Ti and (b) $KZrB_4O_{8.5}$ with a glass-ceramic composition.

fluorescence intensity falls below 10^{-2}. The afterglow time of ZrO_2:Ti was approximately 20 s. Conversely, $KZrB_4O_{8.5}$ with a glass-ceramic composition exhibited an afterglow that was 2.5 times longer, lasting approximately 50 s.

Figure 3 depicts the XRD patterns of ZrO_2:Ti and $KZrB_4O_{8.5}$ with a glass-ceramic composition. All XRD peaks observed for ZrO_2:Ti can be attributed to monoclinic zirconia. XRD peaks of monoclinic zirconia were also detected for $KZrB_4O_{8.5}$ with a glass-ceramic composition.

The Zr*3d*-XPS spectra and peak separation results for ZrO_2:Ti and $KZrB_4O_{8.5}$ with a glass-ceramic composition are shown in Figure 4 (a) and (b), respectively. Two XPS peaks were observed in the 180–186 eV range, which is attributed to Zr*3d*.

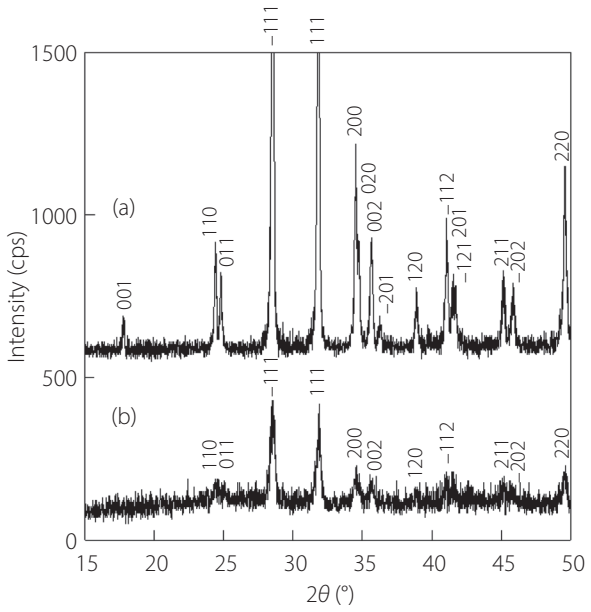

Figure 3: XRD patterns of (a) ZrO_2:Ti and (b) $KZrB_4O_{8.5}$ with a glass-ceramic composition

Note: Numbers represent miller indices of monoclinic ZrO_2 reported in ICDD No. 37-1484.

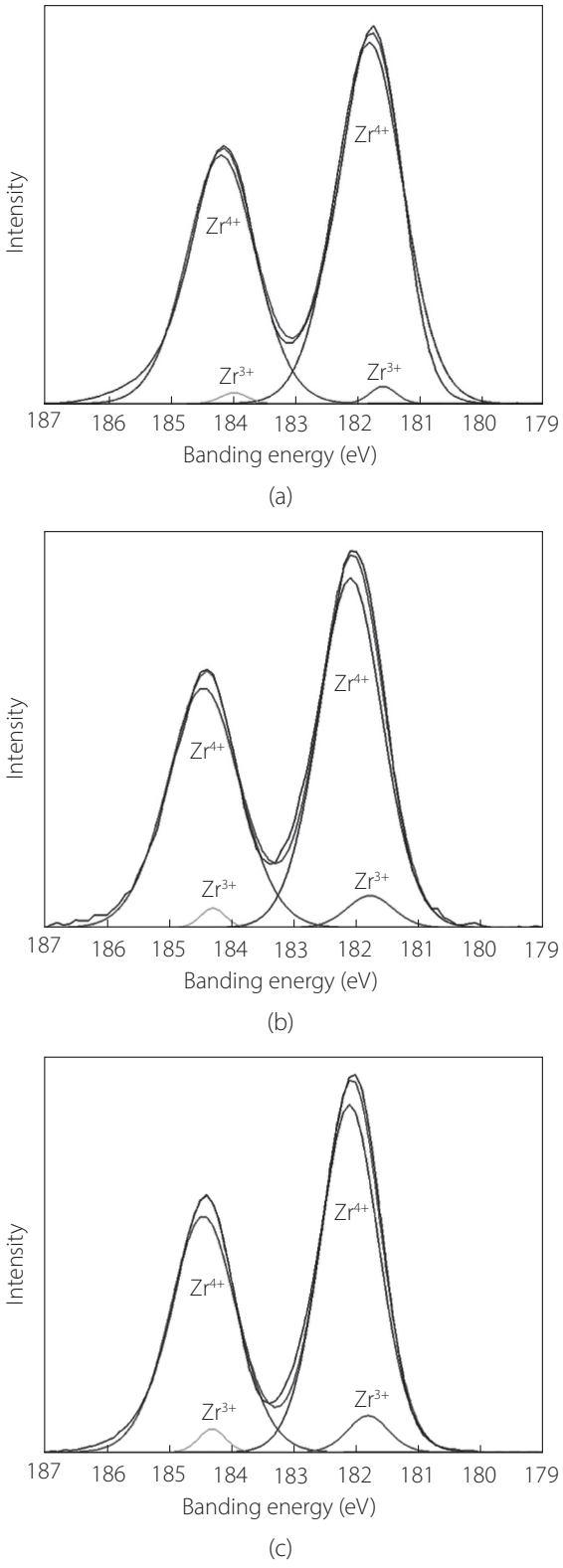

Figure 4: XPS Zr*3d* spectra and peak separation

Note: (a) ZrO_2:Ti, (b) $KZrB_4O_{8.5}$ with a glass-ceramic composition, and (c) ZrO_2:Ti(R).

Two peaks were obtained for each peak through peak separation treatment. The larger peak is assumed to indicate the Zr^{4+} state, and the smaller peak represents the Zr^{3+} state (Bespalov et al., 2015; Huang et al., 2021). However, the Zr^{2+} state, as discussed on the long afterglow mechanism of high-purity ZrO_2 (Iwasaki et al., 2018), was not confirmed via the XPS analysis in this study. The atomic ratios of Zr^{3+}/Zr^{4+} calculated from the peak areas of the separation processed Zr^{4+} and Zr^{3+} were 1.8/98.2 and 4.8/95.2 for ZrO_2:Ti and $KZrB_4O_{8.5}$ with a glass-ceramic composition, respectively. For comparison, Figure 4 (c) shows the Zr*3d*-XPS spectra and peak separation result for ZrO_2:Ti (R), which was reduced through heat treatment at 1350 °C in 3% H_2 (N_2 balance) with ZrO_2:Ti heat-treated at 1500 °C in air. Although the atomic ratio of Zr^{3+}/Zr^{4+} for ZrO_2:Ti (R) was 5.5/94.5, the afterglow time of ZrO_2:Ti and ZrO_2:Ti (R) was almost the same. No correlation was found between their afterglow times and the abundance of Zr^{3+}. Long afterglow is reportedly improved by changing Ti valence from +4 to +3 in ZrO_2:Ti containing 0.1 wt% TiO_2 (Wang et al., 2012). Ti*2p*-XPS spectra were measured in the range of 450–472 eV with an integration frequency of 256; however, the small amount of Ti content prevented accurate XPS peak analysis due to the large influence of noise in this study.

Figure 5 shows reflection electron images of ZrO_2:Ti powder and fracture surface of $KZrB_4O_{8.5}$ with a glass-ceramic composition. The ZrO_2:Ti particles exhibited a uniform size of approximately 0.5 μm. Conversely, in $KZrB_4O_{8.5}$ with a glass-ceramic composition, coarsened grains, roughly 10 μm in size, were detected. An EDS analysis revealed that these grains were primarily composed of B, Zr and O within the potassium borate glass had advanced. The EDS analysis also detected Al; however, this is attributed to the presence of leached aluminous crucibles eroded by the potassium borate glass. The afterglow time of $KZrB_4O_{8.5}$ with a glass-ceramic composition is approximately 2.5 times longer than that of ZrO_2:Ti, as shown in Figure 2.

The afterglow decay curves of $KZrB_2O_{5.5}$, $KZrB_3O_{7.0}$, $KZrB_5O_{10.0}$, and $KZrB_6O_{11.5}$ with a glass-ceramic composition, with varying B content of $KZrB_4O_{8.5}$ with a glass-ceramic composition, are shown in Figure 6. The afterglow time increased in the order of $KZrB_2O_{5.5}$, $KZrB_3O_{7.0}$, and $KZrB_4O_{8.5}$ with a glass-ceramic composition, and decreased for $KZrB_5O_{10.0}$ and $KZrB_6O_{11.5}$ with a glass-ceramic composition. Figure 7 displays the reflected electron images of the fractured surfaces of $KZrB_2O_{5.5}$, $KZrB_3O_{7.0}$, $KZrB_4O_{8.5}$, $KZrB_5O_{10.0}$, and $KZrB_6O_{11.5}$ with a glass-ceramic composition. Coarse grains were observed in all samples, with larger sizes found in $KZrB_3O_{7.0}$ and $KZrB_4O_{8.5}$ with a glass-ceramic composition, and slightly smaller sizes in $KZrB_2O_{5.5}$, $KZrB_5O_{10.0}$, and $KZrB_6O_{11.5}$ with a glass-ceramic composition. This trend in size is consistent with the afterglow time, suggesting that the coarse grain size affects the afterglow characteristics. For instance, it was reported that the afterglow lifetime of $SrAl_2O_4$: Eu^{2+}, Dy^{3+} exhibits higher characteristics with larger crystal particle size (secondary particle size) (Kuboyama et al., 2018).

The PL and afterglow mechanism of monoclinic ZrO_2:Ti

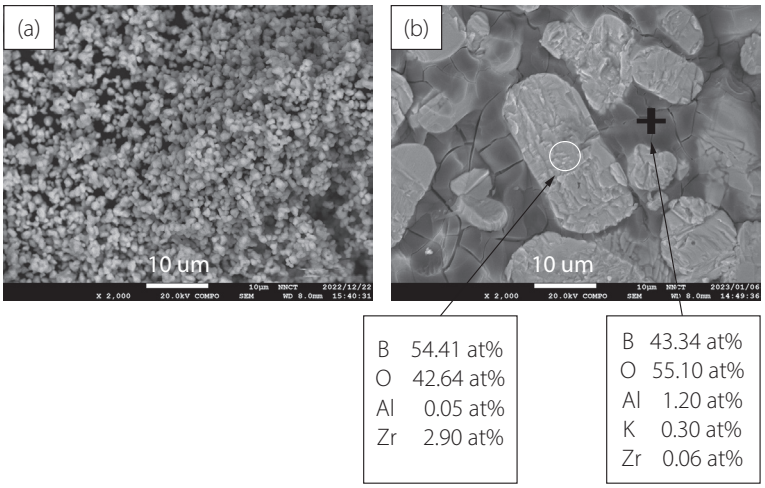

Figure 5: Reflected electron images and point analysis data acquired by EDS
Note: (a) ZrO_2:Ti powder and fracture surface of (b) $KZrB_4O_{8.5}$ with a glass-ceramic composition.

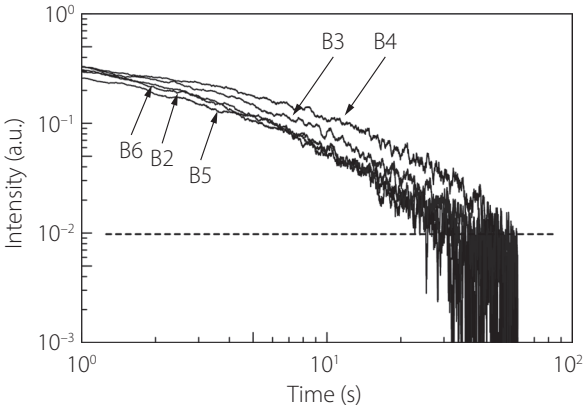

Figure 6: Afterglow decay curves
Note: B2: $KZrB_2O_{5.5}$, B3: $KZrB_3O_{7.0}$, B4: $KZrB_4O_{8.5}$, B5: $KZrB_5O_{10.0}$, and B6: $KZrB_6O_{11.5}$ with a glass-ceramic composition at 475 nm measured by excitation at 280 nm (exposure time: 1 min).

at an excitation wavelength of 300 nm was reported as the scheme in Figure 8 (Carvalho et al., 2012). The bandgap of ZrO_2 is 5.25 eV, and the excitation of electrons from the valance band to the conduction band requires the absorption of UV light ≤ 237 nm. The charge (electron) transfer transition value for Ti–O interactions (e[O(2p)] + $Ti^{IV} \rightarrow Ti^{3+}$) is ≥ 3.72 eV (≤ 333 nm). The excitation of an electron from the t_{2g} ground state of Ti^{3+} to the excited Ti^{IV} + e^- state or the e_g of Ti^{3+} requires the absorption of UV light ≥ 3.47 eV (≤ 357 nm). The difference between these two energy levels is rather small, and the excited levels of Ti^{3+} and Ti^{IV} are situated close to or even within the conduction band. The electrons can easily be promoted from the excited Ti levels to the conduction band of ZrO_2 and can then move further quite freely to the oxygen vacancies (V_o) and be trapped. On the contrary, owing to the absorption of thermal energy, the electrons escape back to the conduction band and populate the emitting level of Ti^{3+} (partially overlapping the conduction band of ZrO_2). The radiative relaxation of the system is considered as the PL (2.47 eV, 500 nm) and afterglow. The bright blue broad band emission at approximately 500 nm is attributed to the Ti^{3+} $3d^1(e_g) \rightarrow 3d^1(t_{2g})$ transition.

In the future, we aim to clarify the mechanism responsible for the coarse grain growth and the effect of coarse grains on improving the afterglow property.

4. Conclusion

The study investigated the improvement of the afterglow property of ZrO_2 containing 1000 ppm TiO_2, (ZrO_2:Ti), which exhibits strong blue emission. ZrO_2:Ti was heat-treated at 1500 °C in the air. The afterglow time of $KZrB_4O_{8.5}$ with a glass-ceramic composition, which is obtained by melting and heat-treating ZrO_2:Ti, K_2CO_3, and H_3BO_3 at 1300 °C in air, was approximately 2.5 times longer than that of ZrO_2:Ti. Only monoclinic peaks were observed in ZrO_2:Ti and $KZrB_4O_{8.5}$ with a glass-ceramic composition via XRD analysis. In the XPS analysis of ZrO_2:Ti and $KZrB_4O_{8.5}$ with a glass-ceramic composition, although the presence of Zr^{4+} and a small amount of Zr^{3+} was observed, that of Zr^{2+} could not be confirmed. For ZrO_2:Ti, particles of uniform size of about 0.5 μm were observed. Contrastingly, in $KZrB_4O_{8.5}$ with a glass-ceramic composition, grains coarsened to approximately 10 μm were observed. The coarse grain was composed of B, Zr, and O. A correlation between the afterglow time and coarse grain size was observed when $KZrB_2O_{5.5}$, $KZrB_3O_{7.0}$, $KZrB_5O_{10.0}$, and $KZrB_6O_{11.5}$ with a glass-ceramic composition were prepared with different B contents in $KZrB_4O_{8.5}$ with a glass-ceramic composition.

Acknowledgement

We would also like to thank Daiichi Kigenso Kagaku Kogyo Co. Ltd. for supplying us with SPZ and Editage (www.editage.jp) for English language editing.

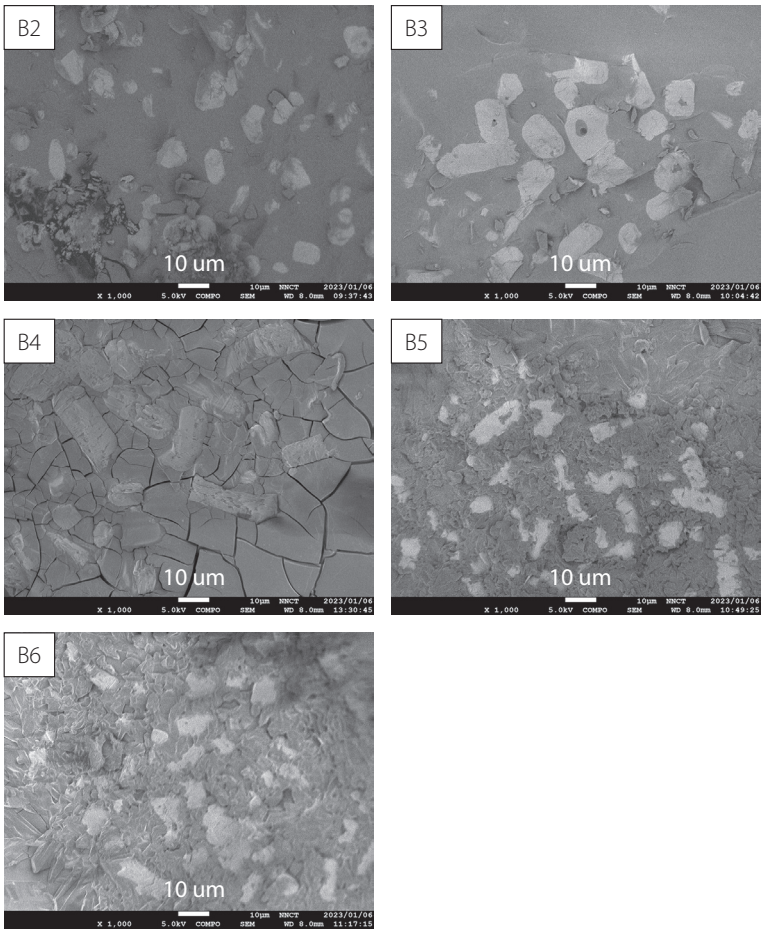

Figure 7: Reflected electron images of fracture surface
Note: B2: $KZrB_2O_{5.5}$, B3: $KZrB_3O_{7.0}$, B4: $KZrB_4O_{8.5}$, B5: $KZrB_5O_{10.0}$, and B6: $KZrB_6O_{11.5}$ with a glass-ceramic composition.

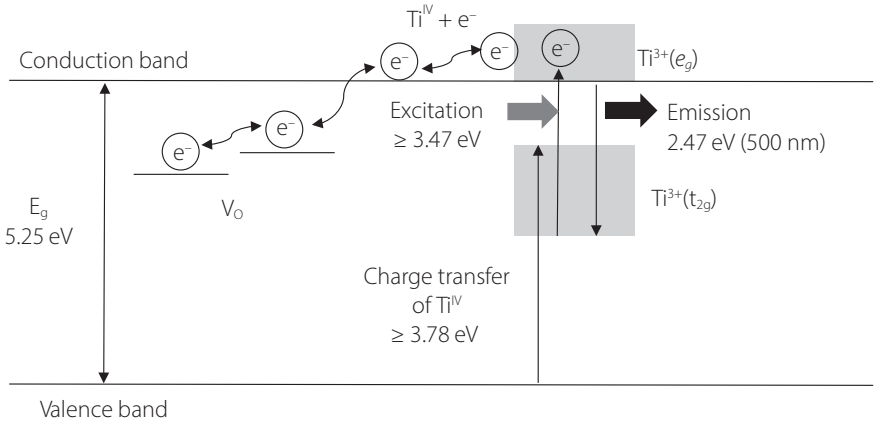

Figure 8: Photoluminescence and afterglow mechanism scheme of ZrO_2:Ti

References

Akiyama, M., Xu, C-N., and Nonaka, K. (2002). Intense visible light emission from stress-activated ZrO_2:Ti. *Applied Physics Letters*, Vol. 81, 457-459.

Iwasaki, K., Takahashi, Y., Terakado, N., Onoue, N., Shinozaki, T., and Fujiwara, T. (2018). Prominent long-lasting photoluminescence in defect-activated zirconia: A rare-earth free and accessible phosphor. *Ceramics International*, Vo. 44, 12929-12933.

Carvalho, J. M., Rodrigues, L. C. V., Hölsä, J., Lastusaari, M., Nunes, L. A. O., Felinto, M. C. F. C., Malta, O. L., and Brito, H. F. (2012). Influence of titanium and lutetium on the persistent luminescence of ZrO_2. *Optical Materials Express*, Vol. 2, 331-340.

Kuboyama, M., Furusawa, H., Mori, D., Takeda, Y., Yamamoto, O., Asahino, K., Kamiya, K., and Imanishi, N. (2018). Effect of alu-

mina sources on the fluorescence properties of long persistent phosphor, $SrAl_2O_4:Eu^{2+}$, Dy^{3+}. *Japan Society of Powder and Powder Metallurgy*, Vol. 65, 176-182. (in Japanese)

Cong, Y., Lia, B., Leia, B., and Li, W. (2007). Long lasting phosphorescent properties of Ti doped ZrO_2. *Journal of Luminescence*, Vol. 126, 822-826.

Sarver, J. F. (1996). Preparation and luminescent properties of Ti-activated zirconia. *Journal of The Electrochemical Society*, Vol. 113, 124-128.

Shimizu, T., Uheda, K., Takizawa, H., Endo, T., and Shimada, M. (1999). Preparation and luminescent properties of MO_2(M=Zr, Hf) with baddeleyite structure. *Japan Society of Powder and Powder Metallurgy*, Vol. 46, 175-179. (in Japanese)

Nakayama, S. and Sakamoto, M. (2016). Fluorescence property of ZrO_2:Ti phosphor and its enhancement in fluorescent intensity by adding phosphorus. *Journal of Materials Research and Technology*, Vol. 5, 289-292.

Nakayama, S., Nitani, I., Asahi, T., Shiomi, M., and Miyata, T. (2016). Synthesis of blue fluorescent ZrO_2:Ti,P/Al_2O_3 composite sintered bodies. *Journal of the Ceramic Society of Japan*, Vol. 124, 950-953.

Hai, O., Jiang, H., Xu, D., and Li, M. (2016). The effect of grain surface on the long afterglow properties of $Sr_2MgSi_2O_7$: Eu^{2+}, Dy^{3+}. *Materials Research Bulletin*, Vol. 76, 358-364.

Huang, J., Liu, J., Tian, L., Li, X., Ma, X., Yu, X., Guo, Q., and Zhao, J. (2021). Ultrathin carbon-coated Zr^{3+}-ZrO_2 nanostructures for efficient visible light photocatalytic antibiotic elimination. *Chemical Engineering Journal*, Vol. 412, 128621.

Bespalov, I., Datler, M., Buhr, S., Drachsel, W., Rupprechter, G., and Suchorski, Y. (2015). Initial stages of oxide formation on the Zr surface at low oxygen pressure: An in situ FIM and XPS study. *Ultramicroscopy*, Vol. 159, 147-151.

Wang, W., Zhang, J., Zheng, G., Liu, Y., and Zhao, Y. (2012). The unusual variations of photoluminescence and afterglow properties in monoclinic ZrO_2 by annealing. *Journal of Luminescence*, Vol. 132, 2817-2821.

(Received: September 20, 2023; Accepted: October 16, 2023)